Robust Artificial Interphases Constructed by a Versatile Protein-Based Binder for High-Voltage Na-Ion Battery Cathodes

Huangxu Li, Chaohong Guan, Jie Zhang, Ke Cheng, Qingxin Chen, Liang He, Xiaochen Ge, Yanqing Lai,* Hongyan Sun,* and Zhian Zhang*

The multiple issues of unstable electrode/electrolyte interphases, sluggish reaction kinetics, and transition-metal (TM) dissolution have long greatly affected the rate and cycling performance of cathode materials for Na-ion batteries. Herein, a multifunctional protein-based binder, sericin protein/ poly(acrylic acid) (SP/PAA), is developed, which shows intriguing physiochemical properties to address these issues. The highly hydrophilic nature and strong H-bond interaction between crosslinking SP and PAA leads to a uniform coating of the binder layer, which serves as an artificial interphase on the high-voltage $Na_4Mn_2Fe(PO_4)_2P_2O_7$ cathode material (NMFPP). Through systematic experiments and theoretical calculations, it is shown that the SP/PAA binder is electrochemically stable at high voltages and possesses increased ionic conductivity due to the interaction between sericin and electrolyte anion ClO_4^-, which can provide additional sodium-migration paths with greatly reduced energy barriers. Besides, the strong interaction force between the binder and the NMFPP can effectively protect the cathode from electrolyte corrosion, suppress Mn-dissolution, stabilize crystal structure, and ensure electrode integrity during cycling. Benefiting from these merits, the SP/PAA-based NMFPP electrode displays enhanced rate and cycling performance. Of note, the universality of the SP/PAA binder is further confirmed on $Na_3V_2(PO_4)_2F_3$. It is believed that the versatile protein-based binder is enlightening for the development of high-performance batteries.

1. Introduction

The sodium-ion battery (SIB) has been widely considered as a promising energy storage technology, and electrode materials for sodium storage have been extensively explored over the past decades.[1–4] However, a cathode with high voltage, good stability, and high rate is still difficult to be achieved due to the multiple interrelated issues including unstable electrode/ electrolyte interphases, sluggish reaction kinetics, and transition-metal (TM) dissolution. Typically, the $Na_4Mn_2Fe(PO_4)_2P_2O_7$ (NMFPP) is promising by virtue of its low-cost and high specific energy density that benefited from the contribution of $Mn^{2+}/3^+$ redox, which can offer a high voltage around 4.0 V.[5,6] Whereas, the related Jahn–Teller effect, Mn-dissolution, and poor kinetics also lead to inferior rate performance and cycling stability of the Mn-dominated material.[7,8]

Many efforts have been devoted to addressing these problems, however, it remains difficult to kill all birds with one stone. Generally, reducing particle size can significantly improve reaction kinetics of electrode materials by shortening Na^+-ion-migration length, while it exacerbates TM-dissolution because a larger surface area of the active material is exposed to electrolyte.[9–12] Although surface coating with oxides/fluorides (e.g., Al_2O_3, TiO_2, AlF_3) may mitigate TM-dissolution and create an artificial barrier for electrolyte oxidation, it causes reduced reaction kinetics because of the limited ionic conductivity and also increases the complexity of mass production process.[12–15] In contrast to the enormous investigation on electrode materials, binder attracts limited attention for SIBs, but the development of binders can be a more direct and feasible strategy to overcome the above challenges of cathodes. As another important component in battery systems, binder integrates the active material, conductive carbon, and current collector, playing a vital role for the final performance of the SIB.[16,17] A binder with high surface coverage, strong adhesion ability, good Na^+ ions conductivity, and high resistance to oxidation is expected to greatly improve electrochemical performance of cathodes. Nevertheless, polyvinylidene fluoride (PVDF), the most widely used

H. Li, J. Zhang, K. Cheng, Q. Chen, H. Sun
Department of Chemistry and COSDAF (Centre of Super-Diamond and Advanced Films)
City University of Hong Kong
83 Tat Chee Avenue, Kowloon, Hong Kong 999077, China
E-mail: hongysun@cityu.edu.hk

H. Li, L. He, X. Ge, Y. Lai, Z. Zhang
School of Metallurgy and Environment
Engineering Research Center of the Ministry of Education for Advanced Battery Materials
Hunan Provincial Key Laboratory of Nonferrous Value-Added Metallurgy
Central South University
Changsha 410083, P. R. China
E-mail: laiyanqing@csu.edu.cn; zhangzhian@csu.edu.cn

C. Guan
University of Michigan–Shanghai Jiao Tong University Joint Institute
Shanghai Jiao Tong University
Shanghai 200240, P. R. China

The ORCID identification number(s) for the author(s) of this article can be found under https://doi.org/10.1002/adma.202202624.

binder for cathode material, hardly to meet all these requirements. Since it is an insulator polymer with low ionic conductivity, PVDF introduces additional high energy barrier for sodium migration at the electrode/electrolyte interphase and leads to deteriorative reaction kinetics. Besides, the weak Van der Waals' force interaction between PVDF and active material, and swelling/softening of PVDF in electrolytes, makes the electrode unstable and damages cycling stability.[18–20] What need to mention is, the use of PVDF is accompanied with *N*-methyl-2-pyrrolidone (NMP) solvent, which is volatile and causes pollution to environment. Water-soluble binders such as poly(acrylic acid) (PAA), carboxymethyl cellulose (CMC), and sodium alginate are more eco-friendly, and by virtue of their abundant carboxymethyl functional groups with strong binding ability, they have been deeply studied to improve cycling stability of many anode materials with large volume changes.[21–24] Nevertheless, only strong binding ability is far from settling the many issues of cathode materials that associate with reaction kinetics, interphase stability, and compositional stability. Besides, binders for cathodes should also possess high electrochemical stability under high voltages. Therefore, a multifunctional binder is highly desired to be developed.

Sericin protein (SP) is a promising biomaterial that exists in silk cocoons and it serves as a natural binder to glue the fibroin fibers together.[25] The polypeptide backbone with rich polar side groups (amino, carboxyl, and hydroxyl) endow sericin good solubility in water and hydrophilicity. Meanwhile, these diverse functional groups and the residue groups of the side chains in amino acid units may endow SP multifunctions (**Figure 1**a). Moreover, SP was reported to show good resistance to oxidation in electronic/electrochemical devices, making it an electrochemically stable binder candidate.[26–28] On the basis of these prominent properties of SP, we judiciously designed a SP-based water-soluble multifunctional binder which is composed of H-bond interconnected SP and polyacrylic acid (PAA). The multi-issues of NMFPP that previously discussed make the material an ideal platform to check the effectiveness of the binder. Through systematic experiments and theoretical calculations, we show that the SP/PAA binder can uniformly cover on the surface of NMFPP and serve as a robust artificial interphase, which is electrochemically inert at high voltage and can effectively protect the NMFPP cathode from Mn-dissolution and mitigate self-discharging. Besides, comparing to PVDF, the SP/PAA possess higher ionic conductivity to boost Na$^+$-ion diffusion, stronger binding capacity to ensure structural integrity, resulting in a more stable cathode electrolyte interphase. Owing to these merits, the rate performance and cycling stability of the SP/PAA-based NMFPP electrode are greatly enhanced.

2. Results and Discussion

The NMFPP was synthesized by a solid-state method. Crystal phase of the material was initially unveiled by X-ray diffraction (XRD) and high-resolution transmission electron microscopy (HRTEM, Figure S1, Supporting Information). The Rietveld refinement identifies that the NMFPP adopts an orthorhombic structure with space group *Pn2₁a*. Lattice structure of the crystalline NMFPP shows clear atomic lattice with interplanar spacing of 0.539 nm, which matches with the (−111) facets of the orthorhombic *Pn2₁a* phase, confirming the successful synthesis of NMFPP. For sericin, its feasibility as a binder was understood by evaluating its physicochemical properties. Chemical structure of SP was studied by X-ray photoelectron spectroscopy (XPS). The three characteristic peaks at 284.80, 286.25, and 288.07 eV in C1s represent C−C, C−O/C=N, and N−C=O/O−C=O bonding structure, respectively (Figure S2a, Supporting Information). And the N1s spectra show two typical peaks of C−NH2 and O=C−N−C at 398.74 and 399.72 eV, respectively (Figure S2b, Supporting Information), which are consistent with the peptide structure of SP.[29,30] The polar groups and small molecule weight endow SP to be easily dissolved in water. Viscosity of SP solution was then studied, and PVDF in NMP solution was also prepared for comparison (Figure 1b). It shows that the viscosity of SP solution is close to water and much smaller than that of PVDF solution. Such low viscosity makes SP difficult to integrate the electrode materials as PVDF. To improve viscosity, water-soluble PAA polymer was added and it shows that the resulting SP/PAA binder solution possessed an enhanced viscosity (38.0 mPa s), which is comparable to PVDF (47.4 mPa s). It is noted that the viscosity of SP/PAA is obviously higher than the calculated value of simple physical mixing, probably due to the H-bonding interaction between the polar groups of SP and PAA.[28] Additionally, the PAA was found to improve film formation property. As shown in Figure S3 (Supporting Information), the segregation of yellow and white components indicates that the as-formed SP film is inhomogeneous. In stark contrast, SP/PAA film is very uniform, which should be benefited from the hydrogen bond interaction within the crosslinking SP/PAA binder.[31] The suitable viscosity and good film formation ability makes SP/PAA an attractive binder for battery electrode. Furthermore, Fourier transform infrared spectroscopy (FTIR) was applied to verify the chemical structure of the binders. As shown in Figure 1c, PAA demonstrates typical peaks at 1162, 1411, and 1709 cm^{-1}, corresponding to C−O stretching, C−O−H in-plane bonding, and C=O stretching, respectively.[32,33] FTIR spectra of SP reveal characteristic peaks at 1507 and 1620 cm^{-1}, corresponding to in-plane N−H bending and C=O stretching vibration, respectively.[34] The broad peak centered at around 3200 cm^{-1} represents O−H stretching. For SP/PAA, it shows characteristic peaks of SP and PAA, indicating the presence of both materials. Notably, the peaks originally located at 1507, 1620, and 1709 cm^{-1} are slightly shifted in SP/PAA. This further confirms the hydrogen bonding interaction between the −NH− group in SP and the −COOH group in of PAA,[35] as illustrated in Figure 1d.

Morphology of the binder has profound impact on electrochemical properties of electrodes. Scanning electron microscopy (SEM) image of the PVDF film revels a porous structure (Figure 1e), which is unfavorable to achieve uniform and intact surface coating of the electrode materials. In contrast, SP and PAA films show improved flatness with no pores (Figure S4, Supporting Information). Moreover, the combined SP/PAA film displays the flattest and smoothest surface among the binder films. Distribution of components of the film is uniform, as C, O, and N are detected and is evenly distributed (Figure 1f). The high-quality film could possibly act as a robust protecting layer for electrode materials (discussed later).
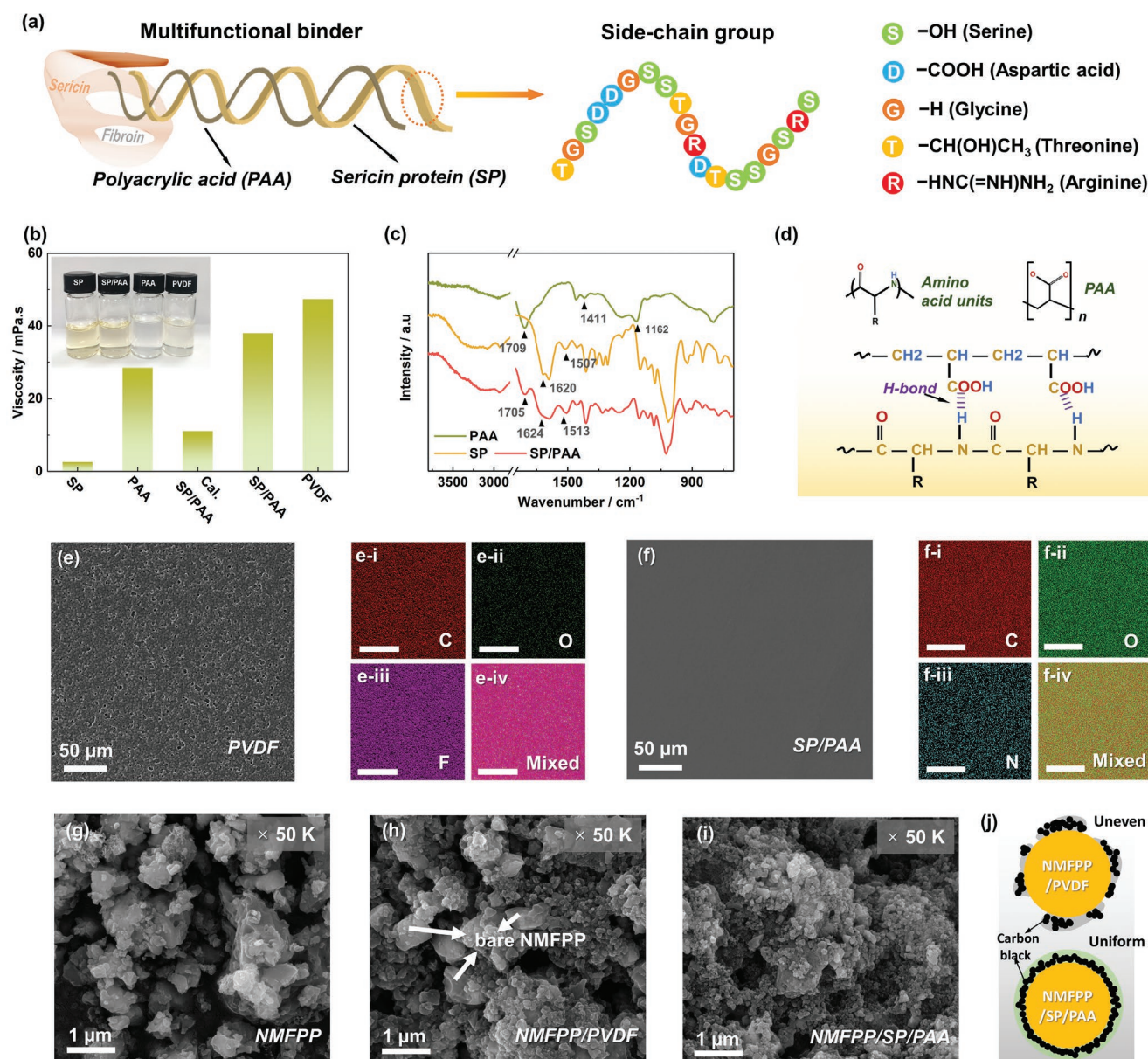
Figure 1. Physicochemical characterization of the NMFPP cathode and the binders. a) Schematic illustration of the multifunctional binder (SP/PAA) that incorporates two functional materials and the chemical structure of sericin. b) The viscosities of SP, PAA, SP/PAA, and PVDF solution (3 wt%) at room temperature; the calculated viscosity of SP/PAA (Cal. SP/PAA) is based on the mass ratio of SP to PAA (2:1). The inset shows photographs of the solutions. c) Fourier transform infrared (FTIR) spectroscopy of PVDF, SP, PAA, and SP/PAA binder films. d) Chemical formula of SP and PAA and schematic illustration of the H-bonding structure between them. e) SEM and elemental mapping images of PVDF films, which show even distribution of C, O, and F. f) SEM and elemental mapping images of SP/PAA films. g–i) SEM images of pure NMFPP (g), NMFPP electrode using PVDF binder (h), and NMFPP electrode using SP/PAA binder (i). j) Schematic illustration of the coating structure of the NMFPP/PVDF electrode and the NMFPP/SP/PAA electrode.

However, the protecting layer should not hinder sodium diffusion process. To understand this, ionic conductivities of the SP/PAA and PVDF films are measured via the resistance tests. Electrochemical impedance spectroscopy (EIS) and calculation process can be seen in Figure S5 (Supporting Information). The calculated ionic conductivity of SP/PAA and PVDF film is 1.96×10^{-7} and 3.2×10^{-8} S cm^{-1} at 25 °C, respectively. The enhanced ionic conductivity of SP/PAA binder should be attributed to its amorphous nature, which was probed by XRD as presented in Figure S6 (Supporting Information). It is believed that the amorphous structure can promote ion movements due to the coordination bonds and easily segmented motion of amorphous sericin unit.[36,37] Electrochemical stability of the binder films under the battery operation conditions was studied by cyclic voltammetry (CV, Figure S7, Supporting Information). Clearly, the PVDF shows higher reaction current than SP/PAA, especially in the high voltage region (>4.0 V) during oxidation, indicating great electrochemical stability of the SP/PAA binder.

**ADVANCED
SCIENCE NEWS**

www.advancedsciencenews.com

**ADVANCED
MATERIALS**

www.advmat.de

Thermal gravimetric analysis (TGA) further demonstrates that SP/PAA binder is thermally stable as an SIB electrode binder, considering that the operation temperature of SIBs is far below the decomposition temperature of SP/PAA (Figure S8, Supporting Information).

Based on the above discoveries, the protein-based binder is expected to improve electrochemical performance of the high voltage NMFPP cathode material. As a proof-of-concept study, the SP/PAA electrode and PVDF electrode were subjected to rate performance and cycling stability tests. First, morphologies of the electrodes were studied by SEM (Figure 1g–i) and TEM (Figure S9, Supporting Information). It can be seen that the SP/PAA binder leads to homogeneous combination of conductive carbon and NMFPP particles, as the surface of all NMFPP particles is covered by carbon. While the PVDF-based electrode exhibited some bare NMFPP particles without carbon coverage, as illustrated in Figure 1j. The hydrophilic nature, suitable viscosity, and good film formation of SP/PAA binder are the keys to the thorough mixing of electrode components, and the uniform surface is beneficial to the electrochemical performance of NMFPP.

Figure 2a,b shows the rate performance and the corresponding discharge curves of the electrodes from 0.1 to 2 C. Obviously, the SP/PAA-based electrode displays better rate capability than that of PVDF electrode at different current densities. Given that the NMFPP particles synthesized by solid-state method are large (Figure S9a, Supporting Information) and without any modification, the enhanced rate performance greatly proves the effectiveness of the protein-based binder. Additionally, peaks of CV curves for the SP/PAA electrode were found left-shifted during oxidation and right-shifted during reduction, indicating that the SP/PAA-based electrode has reduced polarization (Figure 2c). This should be ascribed to the high ionic conductivity of SP/PAA film, which helps to increase the apparent sodium-diffusion coefficients of the electrode, as revealed by the galvanostatic intermittent titration technique (GITT, Figure S10, Supporting Information). To show the importance of SP for the enhanced performance, electrochemical performance of pure PAA-based electrode was also studied. Of note, the PAA-based electrode demonstrates the poorest rate performance among the electrodes due to the huge polarization, as
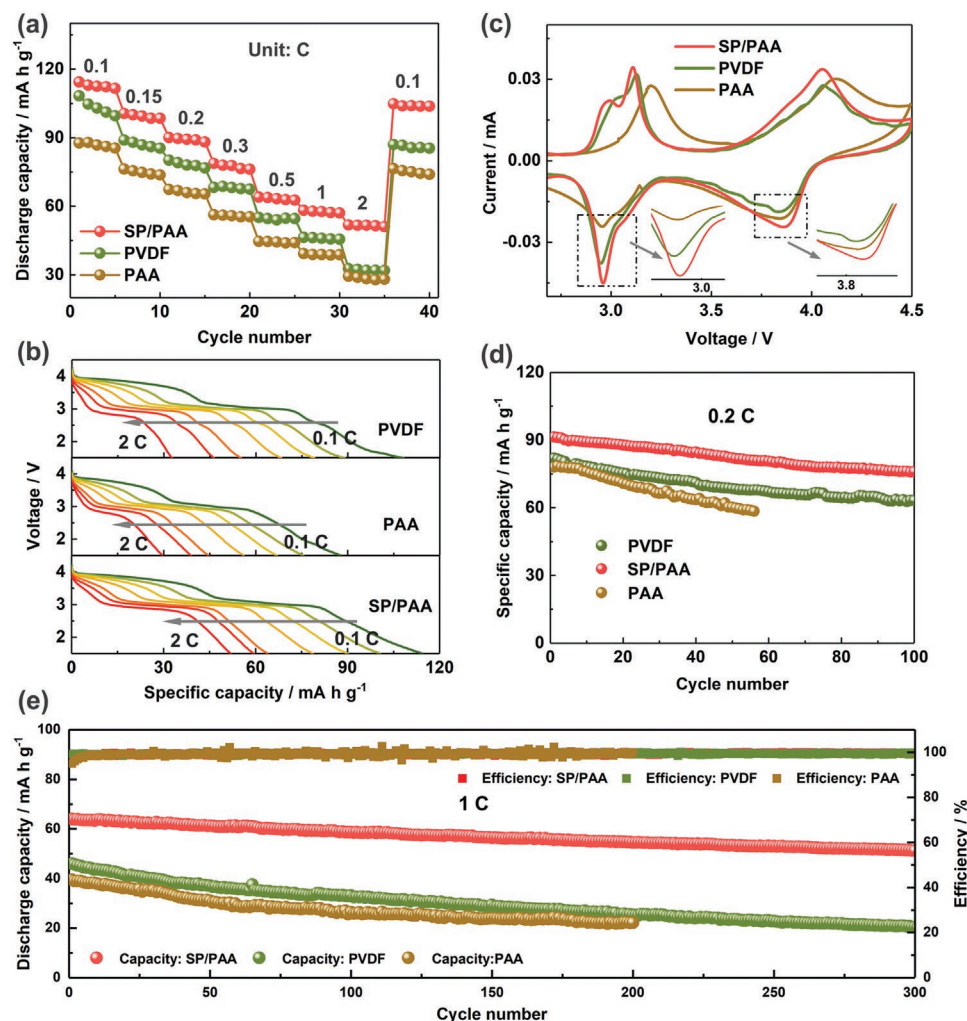

Figure 2. Electrochemical performance of NMFPP electrodes made up from different binders. a) Rate performance of the electrodes from 0.1 to 2 C. b) The corresponded discharge profiles at different rates. c) Cyclic voltammetry (CV) curves at the scan rate of 0.1 mV s⁻¹. d) Cycling performance at low rate of 0.2 C. e) Cycling performance at high rate of 1 C.

observed in the CV curves. The huge polarization also leads to fast capacity decay during cycling. As demonstrated in Figure 2d and Figure S11a (Supporting Information), capacity of the PAA-based electrode decreases rapidly and merely 74.8% of its initial capacity is obtained after 56 cycles at 0.2 C. While for the SP/PAA-based electrode, it delivers an initial capacity of 91.4 mA h g^{-1} and a capacity retention of 83.2% after 100 cycles, which is also significantly higher than that of the PVDF-based electrode (77.2%). Therefore, SP does play a key role to the enhanced electrochemical performances of the SP/PAA-based electrode. Even under the elevated current density (1 C), the SP/PAA-based electrode can remain 79.8% of its initial capacity after 300 cycles, in remarkable contrast to the 44.4% of PVDF-based electrode (Figure 2e and Figure S11b, Supporting Information).

The superior electrochemical performance of SP/PAA against PVDF as a binder and the key role that SP has presented motivates us to further investigate the underlining mechanism. Considering the fundamental impact of reaction kinetics, sodium-ion diffusion behavior in the binder was primarily studied by DFT calculations. Previous study on protein-based solid-state electrolyte has discovered that positively charged side groups of specific amino acids (e.g., arginine, histidine, and lysine) can adsorb ClO_4^- anion in the battery electrolyte by electrostatic interactions and thus affects lithium-ion diffusion.[38,39] Inspired by this finding, three peptide chains using arginine, histidine, and lysine as the building blocks were constructed by dehydration condensation to have a clue of sodium-ion diffusion in sericin protein (Figure S12, Supporting Information). DFT fully relaxed constructed models consisting of one peptide chain and one free ClO_4^- anion close to the positively charged group in a vacuum space are shown in Figure S13 (Supporting Information). Based on these structures, it was found that Na$^+$ prefers to be attracted by oxygen of the peptide chains (Figure S14, Supporting Information). The climbing image nudged elastic band method (CI-NEB) was then employed to study the migration energy pathways of sodium. As shown in **Figure 3**, it can be found that the existence of ClO_4^- group provides additional Na$^+$ coordinating sites (Na3), which lead to new diffusion paths of Na1–Na3–Na2 in the three types of peptide chains with ClO_4^- (Figure 3a–f). Besides, the diffusion path of Na1–Na3–Na2 in the three peptide chains demonstrates much smaller Na-diffusion energy barriers (0.06–0.23 eV) than that of Na1-Na2 paths in peptide chains without ClO_4^- (0.7–0.88 eV), as exhibited in Figure 3g–i. This could be a reason for the high ionic conductivity of the SP-based binder and good rate performance of the electrode.

The stability of the binder during battery operation is key to keep electrode structure intact and thus avoid fast capacity
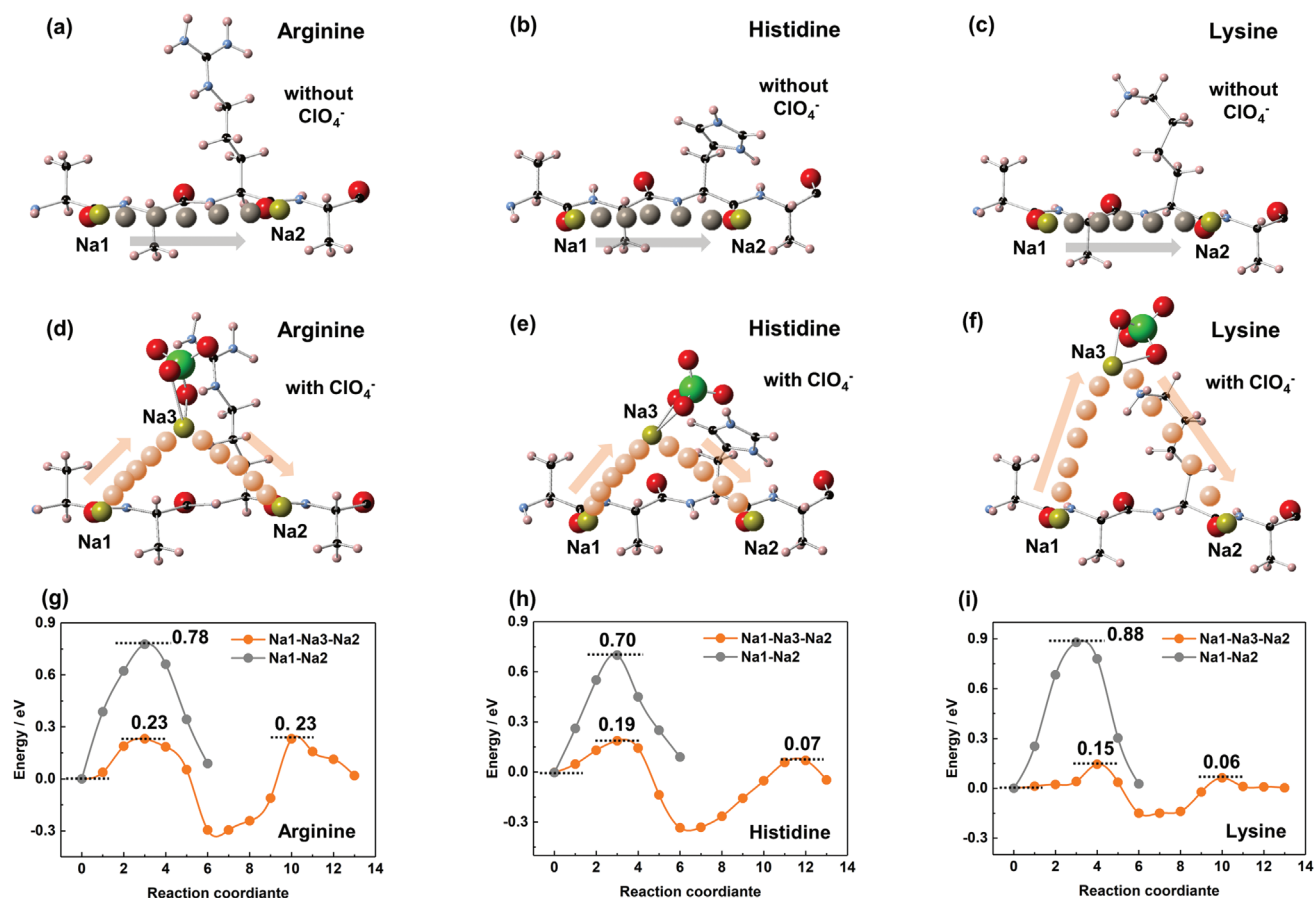

Figure 3. DFT calculations disclose the effect of SP on the enhanced sodium storage performance. a–c) Na$^+$-ion diffusion paths in arginine (a), histidine (b), and lysine (c), without the ClO_4^-. d–f) Na$^+$-ion diffusion paths in arginine (d), histidine (e), and lysine (f) with the existence of ClO_4^-. g–i) Sodium diffusion energy barriers in arginine (g), histidine (h), and lysine (i).

**ADVANCED
SCIENCE NEWS**

www.advancedsciencenews.com

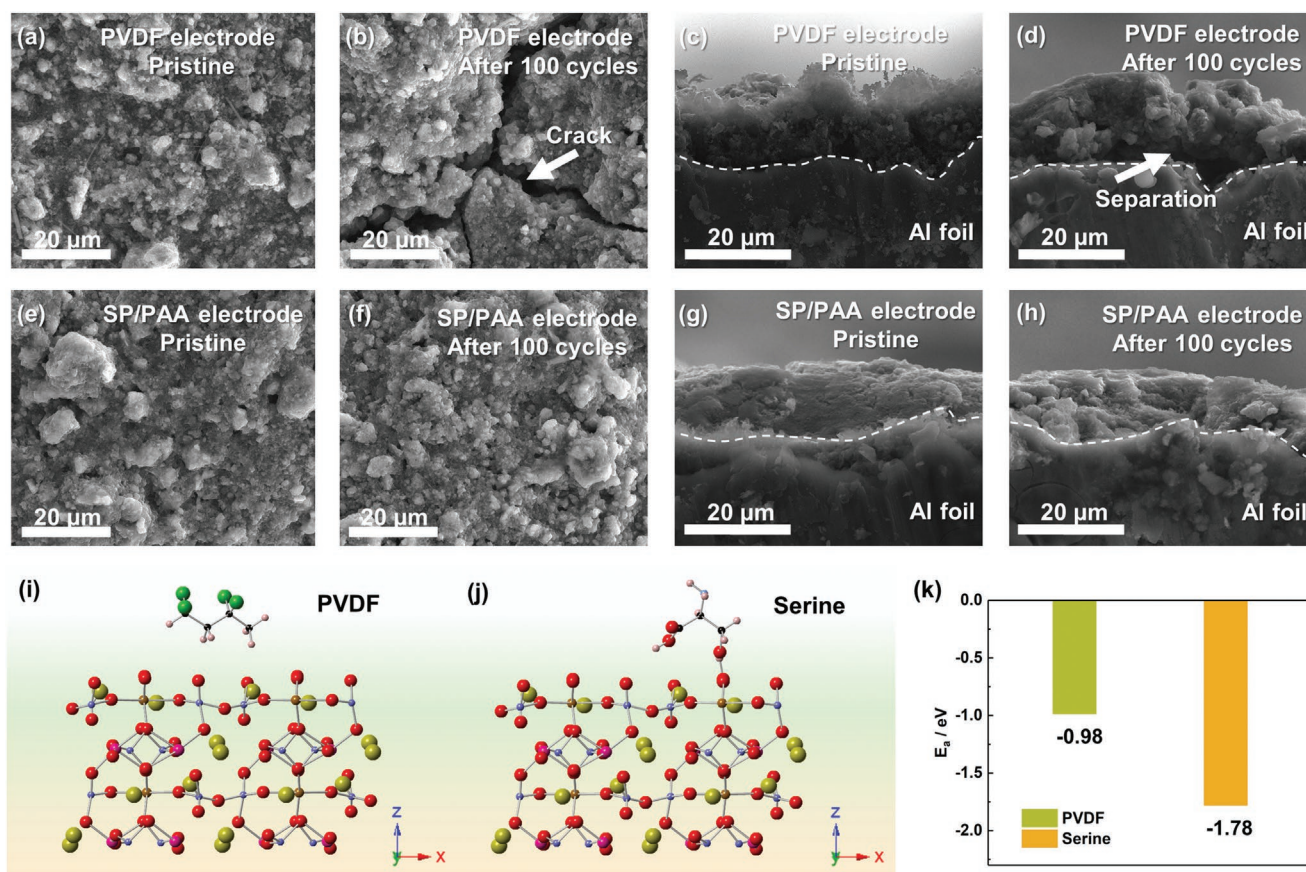**ADVANCED
MATERIALS**

www.advmat.de

Figure 4. Integrity of the electrodes. a,b) SEM images of the pristine material (a) and after 100 cycles (b) for the PVDF electrodes. c,d) The corresponding cross sections of the PVDF electrodes. e,f) SEM images of the pristine material (e) and after 100 cycles (f) for the SP/PAA electrodes. g,h) The corresponding cross sections of the SP/PAA electrodes. i,j) Adsorption configurations of PVDF (i) and serine (j) on the $Na_4Mn_2Fe(PO_4)_2P_2O_7$ (001) crystal plane. Red, green, black, pink, blue, purple, brown, rosy, and yellow spheres represent O, F, C, H, N, P, Fe, Mn, and Na atoms, respectively. k) Calculated adsorption energy.

decay. To understand it, the structure evolution of the electrodes before and after cycling at 0.2 C was studied by SEM. As shown in **Figure 4**a,b, several cracks are generated in PVDF electrode after 100 cycles. And from the cross-section images (Figure 4c,d), clear separation between the electrode materials and Al current collector is observed after cycling. In contrast, no cracks or separation is found in the SP/PAA electrode, manifesting the great binding ability of the SP/PAA to integrate the electrode, and thus mitigate capacity decay during cycling (Figure 4e–h). Stretch tests of adhesive force confirm the strong interaction between SP/PAA binder and the current collector (Al foil) as the peeling-off force of SP/PAA electrode is higher than that of PVDF electrode (Figure S15, Supporting Information). Meanwhile, the interactions between the binder and the NMFPP active material is also important, and it was studied by theoretical calculating adsorption energies between the binders and NMFPP. To simplify the calculation process, serine, the most important component in sericin, and a typical fragment of PVDF were used for calculation (Figure S16, Supporting Information). The atomic structure of binders on $Na_4Mn_2Fe(PO_4)_2P_2O_7$ (001) after adsorption is illustrated in Figure S17 (Supporting Information), and the most stable configurations are shown in Figure 4i,j. Obviously, the PVDF

is relatively far away from the surface of $Na_4Mn_2Fe(PO_4)_2P_2O_7$ (H−O distance: 2.41 Å), indicating a weak interaction force. While the hydroxide group in serine tends to closely interact with the surface oxygen of $Na_4Mn_2Fe(PO_4)_2P_2O_7$ (H−O distance: 1.43 Å), manifesting strong hydrogen bonding interactions.[19] Besides, Figure 4k shows that the adsorption energy of PVDF and serine on $Na_4Mn_2Fe(PO_4)_2P_2O_7$ (001) is −0.98 and −1.78 eV, respectively, confirming the stronger interactions between sericin and NMFPP.

Besides electrode kinetics and integrity, electrode/electrolyte interphases, which usually form on a cathode surface during oxidation process, also have profound impact on cycling stability of electrodes.[40] To understand the effect of binders on interphase, evolution of interfaces during cycling was studied by XPS (**Figure 5**a,b). Comparing the C1s spectra of the two pristine electrodes, significant increase of the peak at 289.5–289.8 eV, which corresponds to Na_2CO_3 and $ROCO_2Na$ species, was found in both electrodes after ten cycles, indicating the formation of cathode electrolyte interphase layer. And the increase of C−O (285.8–286.0 eV), C=O (287.0–287.2 eV), and O=C−O (288.5–288.6 eV) corresponds to decomposition of carbonate-based electrolyte.[41–43] Peaks representing the interphase composition of the 100th cycle SP/PAA electrode was found similar
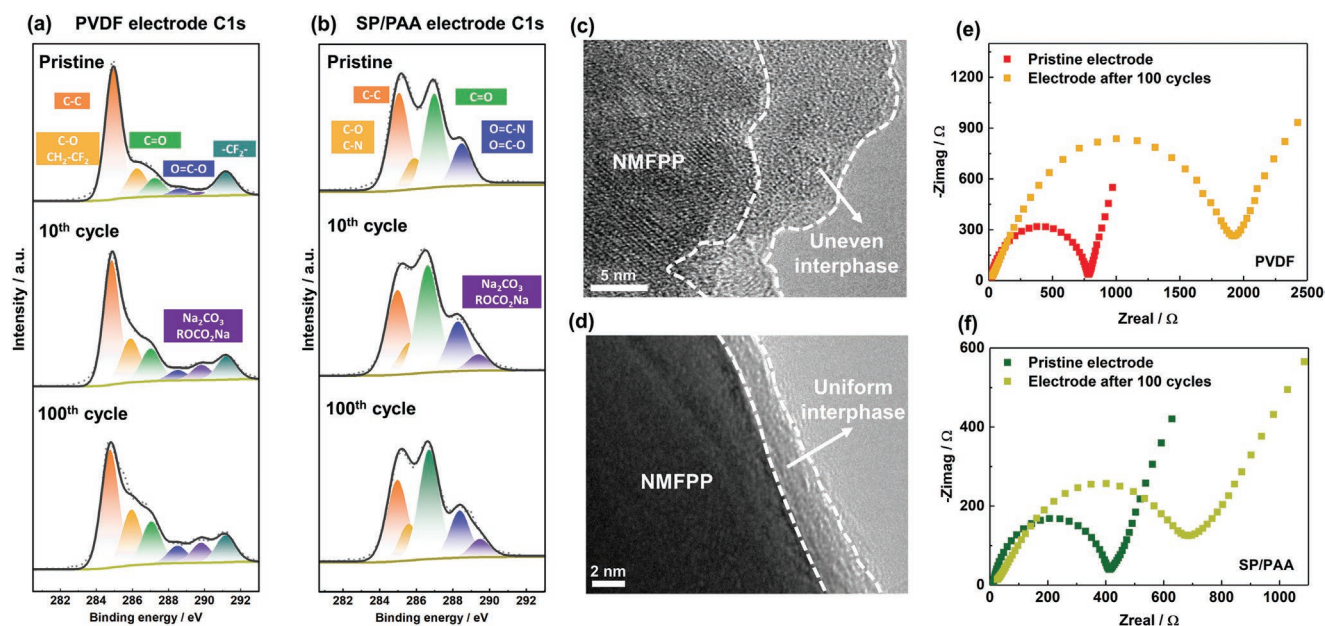
**ADVANCED
SCIENCE NEWS**

www.advancedsciencenews.com

**ADVANCED
MATERIALS**

www.advmat.de

Figure 5. Interphase properties of the electrode. a,b) The surface composition evolution upon cycling disclosed by C 1s high-resolution XPS. c,d) HRTEM images of the PVDF-based (c) and SP/PAA-based (d) NMFPP electrodes after cycling. e,f) EIS of SP/PAA-based (e) and PVDF-based (f) NMFPP electrode measured in half-cell configuration.

to the 10th cycle. While the corresponding peaks continue to increase in the PVDF electrode, manifesting the interphase of SP/PAA electrode is stable but the interphase of PVDF electrode keeps changing. This is further confirmed by analyzing the evolution trend of O 1s (Figure S18, Supporting Information). The unstable interphase of PVDF-based electrode should derive from the unsatisfactory coating effect of PVDF binder, which leads to inhomogeneous reaction environment and fails to avoid continuous electrolyte oxidation. As revealed by HR-TEM (Figure 5c,d), the interphase of PVDF-based electrode is thick and uneven, in stark contrast to the thin and uniform interphase of the SP/PAA-based electrode. The stable uniform interphase is believed to ameliorate the reaction kinetics of the electrode. As shown in Figure 5e,f and Figure S19 (Supporting Information), electrochemical impedance spectra (EIS) of PVDF electrode revels a substantial increase of charge-transfer resistance from 783 to 1924 Ω after 100 cycles. While for SP/PAA electrode, the increment of charge-transfer resistance over cycling is much smaller (from 409 to 683 Ω), which is the key to the enhanced cycling performance.

After confirming the stable interphase, the remaining issue is the impact of the binders on the NMFPP active material. The linear long-chain structure, weak interaction force, porous film structure led to poor coverage of PVDF on NMFPP, exposing more NMFPPs to electrolyte. While the intact and smooth SP/PAA binder with good coverage is suggested to act as a robust protecting layer to prevent the active material from unfavorable side reactions. To prove this hypothesis, voltage decay of the batteries against resting time has been monitored (**Figure 6**a). The voltage decay of high voltage cathode materials has been an issue because high voltage can drive continuous electrons flow from the electrolyte to cathode. When the electrodes are charged to 4.5 V, the voltage of PVDF under resting condition falls obviously faster than that of SP/PAA. Severe

self-discharge in PVDF electrode can lead to electrolyte decomposition and cause unstable interphase, which is in agreement with the XPS results. Furthermore, manganese-dissolution, another issue for Mn-based materials, was also studied for the two electrodes (Figure 6b). The electrodes were immersed in electrolyte and resting for 30 d. Inductively coupled plasma (ICP) shows that the concentration of manganese in electrolyte of SP/PAA-based electrode is only 12.4% of the PVDF-based electrode. These results verify that the protein-based binder can effectively prevent electrolyte corrosion and Mn-dissolution, thus improving electrochemical performance of the NMFPP. The crystal structure variations of NMFPP were monitored by ex situ XRD (Figure S20 and Figure 6c,d). The reflection peaks of (200) and (011) has been identified and shows reversible peak-shifting during sodium-ion insertion/extraction. No new peaks appeared during the whole process, indicating a reversible single-phase reaction mechanism as previously reported.[5,44] Of note, the SP/PAA-based electrode shows better stability, as the variation of (200) peak between the fully charged state and fully discharged state for the SP/PAA and PVDF-based electrode is 0.27° and 0.41° respectively. This verifies that the uniformly coated SP/PAA binder and the strong hydrogen-bonding interaction force can protect the NMFPP from side reactions and stabilize NMFPP, therefore resulting in the enhanced cycling stability.[19]

Physiochemical properties of the protein-based binder have been well studied. Comparing to PVDF, the above discussed unique properties endow SP/PAA with multifunctions to overcome the many issues of NMFPP, as summarized in Figure 6e. Based on these functions, the versatile binder is deduced to improve performance of other cathode materials. To verify this hypothesis, $Na_3V_2(PO_4)_2F_3$ (NVPF), a well-studied high voltage cathode material was then synthesized (Figure S21, Supporting Information) and subjected to rate and cycling tests by using SP/PAA and PVDF as the binders. Surprisingly, as shown in
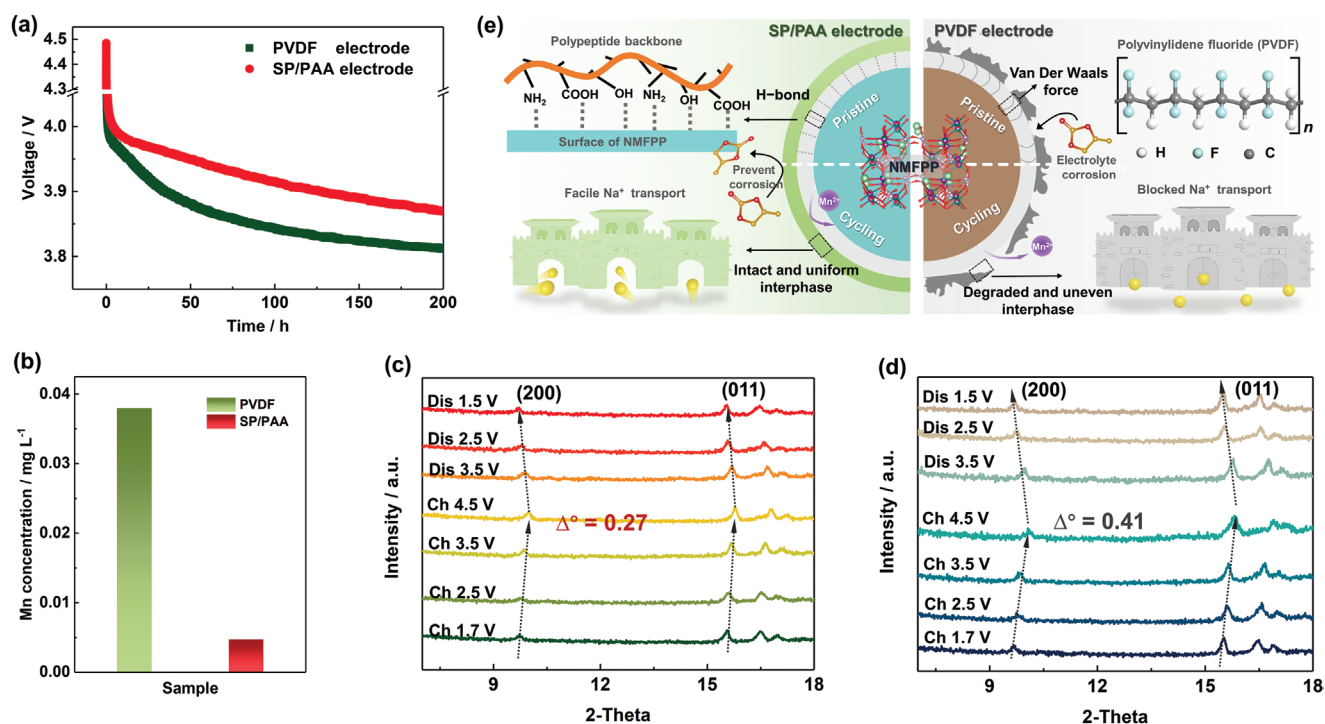
Figure 6. Stability of the electrodes. a) Self-discharging tests of the two electrodes. b) Mn concentration of the electrolytes determined by ICP. c) Ex situ XRD of the SP/PAA electrodes. d) Ex situ XRD of the PVDF electrodes. e) Schematic illustration of the features and functions of SP/PAA and PVDF binders.

Figure S22 (Supporting Information), the SP/PAA-based NVPF cathode exhibits better high-rate and cycling performance than that of the PVDF-based electrode. Considering the NVPF has a higher redox voltage (≈4.1 V) than that of NMFPP, the successful application of SP/PAA binder in NVPF verifies great stability and universality of the protein-based binder, which can be also feasible for many other cathode materials with a general voltage ranging from 2.0 to 4.0 V.

3. Conclusions

A sericin protein-based binder SP/PAA is developed and showed intriguing physicochemical properties as a multifunctional electrode binder. Due to the abundant polar groups of side chains and the hydrophilic property, the SP/PAA binder can uniformly cover on the surface of NMFPP. DFT calculations demonstrate that the interaction force between the SP/PAA binder and NMFPP is much stronger than that of the PVDF, which endows great structural integrity of the SP/PAA electrode for cycling. Besides, the interaction between protein and ClO_4^- anion groups is found to provide additional sodium diffusion paths with reduced energy barriers, resulting in enhanced ionic conductivity for fast sodium migration. Moreover, the uniformly coated binder film serves as a robust artificial interphase, which helps to stabilize the cathode electrolyte interface, and protect the NMFPP cathode from electrolyte corrosion and Mn-dissolution. The versatile protein-based binder offers new opportunities to improve the electrochemical performance of battery electrode materials.

Supporting Information

Supporting Information is available from the Wiley Online Library or from the author.

Conflict of Interest

The authors declare no conflict of interest.

Data Availability Statement

The data that support the findings of this study are available from the corresponding author upon reasonable request.

**ADVANCED
SCIENCE NEWS**

www.advancedsciencenews.com

**ADVANCED
MATERIALS**

www.advmat.de

[1] N. Yabuuchi, K. Kubota, M. Dahbi, S. Komaba, *Chem. Rev.* **2014**, *114*, 11636.

[2] J. Peng, W. Zhang, Q. Liu, J. Wang, S. Chou, H. Liu, S. Dou, *Adv. Mater.* **2022**, *34*, 2108384.

[3] Y. J. Guo, P. F. Wang, Y. B. Niu, X. D. Zhang, Q. Li, X. Yu, M. Fan, W. P. Chen, Y. Yu, X. Liu, Q. Meng, S. Xin, Y. X. Yin, Y. G. Guo, *Nat. Commun.* **2021**, *12*, 5267.

[4] T. Jin, H. Li, K. Zhu, P. F. Wang, P. Liu, L. Jiao, *Chem. Soc. Rev.* **2020**, *49*, 2342.

[5] H. Kim, G. Yoon, I. Park, J. Hong, K. Y. Park, J. Kim, K. S. Lee, N. E. Sung, S. Lee, K. Kang, *Chem. Mater.* **2016**, *28*, 7241.

[6] H. Li, M. Xu, Z. Zhang, Y. Lai, J. Ma, *Adv. Funct. Mater.* **2020**, *30*, 2000473.

[7] H. Kim, G. Yoon, I. Park, K. Y. Park, B. Lee, J. Kim, Y. U. Park, S. K. Jung, H. D. Lim, D. Ahn, S. Lee, K. Kang, *Energy Environ. Sci.* **2015**, *8*, 3325.

[8] H. Li, W. Zhang, K. Sun, J. Guo, K. Yuan, J. Fu, T. Zhang, X. Zhang, H. Long, Z. Zhang, Y. Lai, H. Sun, *Adv. Energy Mater.* **2021**, *11*, 2100867.

[9] T. Wang, W. Zhang, H. Li, J. Hu, Y. Lai, Z. Zhang, *ACS Appl. Energy Mater.* **2020**, *3*, 3845.

[10] H. Pan, X. Lu, X. Yu, Y. S. Hu, H. Li, X. Q. Yang, L. Chen, *Adv. Energy Mater.* **2013**, *3*, 1186.

[11] Q. Wei, X. Chang, J. Wang, T. Huang, X. Huang, J. Yu, H. Zheng, J. H. Chen, D. L. Peng, *Adv. Mater.* **2022**, *34*, 2108304.

[12] C. Zhan, T. Wu, J. Lu, K. Amine, *Energy Environ. Sci.* **2018**, *11*, 243.

[13] Y. Zhang, J. Zhang, X. Li, G. Chen, B. Zhang, H. Liu, Y. Wang, Z. F. Ma, *Chem. Eng. J.* **2022**, *430*, 132708.

[14] J. W. Kim, D. H. Kim, D. Y. Oh, H. Lee, J. H. Kim, J. H. Lee, Y. S. Jung, *J. Power Sources* **2015**, *274*, 1254.

[15] C. Zhang, X. Liu, Q. Su, J. Wu, T. Huang, A. Yu, *ACS Sustainable Chem. Eng.* **2016**, *5*, 640.

[16] R. R. Li, Z. Yang, X. X. He, X. H. Liu, H. Zhang, Y. Gao, Y. Qiao, L. Li, S. L. Chou, *Chem. Commun.* **2021**, *57*, 12406.

[17] H. Wang, B. Wu, X. Wu, Q. Zhuang, T. Liu, Y. Pan, G. Shi, H. Yi, P. Xu, Z. Xiong, S. L. Chou, B. Wang, *Small* **2022**, *18*, 2101680.

[18] J. T. Li, Z. Y. Wu, Y. Q. Lu, Y. Zhou, Q. S. Huang, L. Huang, S. G. Sun, *Adv. Energy Mater.* **2017**, *7*, 1701185.

[19] H. Huang, Z. Li, S. Gu, J. Bian, Y. Li, J. Chen, K. Liao, Q. Gan, Y. Wang, S. Wu, Z. Wang, W. Luo, R. Hao, Z. Wang, G. Wang, Z. Lu, *Adv. Energy Mater.* **2021**, *11*, 2101864.

[20] J. Zhao, X. Yang, Y. Yao, Y. Gao, Y. Sui, B. Zou, H. Ehrenberg, G. Chen, F. Du, *Adv. Sci.* **2018**, *5*, 1700768.

[21] S. Choi, T. W. Kwon, A. Coskun, J. W. Choi, *Science* **2017**, *357*, 279.

[22] Z. Ma, Y. Lyu, H. Yang, Q. Li, B. Guo, A. Nie, *J. Power Sources* **2018**, *401*, 195.

[23] T. W. Kwon, J. W. Choi, A. Coskun, *Chem. Soc. Rev.* **2018**, *47*, 2145.

[24] D. Kim, C. Hwang, J. Jeong, W. J. Song, S. Park, H. K. Song, *ACS Appl. Mater. Interfaces* **2019**, *11*, 43039.

[25] X. Liang, H. Li, J. Dou, Q. Wang, W. He, C. Wang, D. Li, J. M. Lin, Y. Zhang, *Adv. Mater.* **2020**, *32*, 2000165.

[26] H. Wang, Y. Du, Y. Li, B. Zhu, W. R. Leow, Y. Li, J. Pan, T. Wu, X. Chen, *Adv. Funct. Mater.* **2015**, *25*, 3825.

[27] H. Wang, F. Meng, Y. Cai, L. Zheng, Y. Li, Y. Liu, Y. Jiang, X. Wang, X. Chen, *Adv. Mater.* **2013**, *25*, 5498.

[28] J. Liu, D. G. D. Galpaya, L. Yan, M. Sun, Z. Lin, C. Yan, C. Liang, S. Zhang, *Energy Environ. Sci.* **2017**, *10*, 750.

[29] H. Wu, Q. Wu, F. Chu, J. Hu, Y. Cui, C. Yin, C. Li, *J. Power Sources* **2019**, *419*, 72.

[30] W. Li, Z. Zhang, B. Kong, S. Feng, J. Wang, L. Wang, J. Yang, F. Zhang, P. Wu, D. Zhao, *Angew. Chem.* **2013**, *52*, 8151.

[31] Y. Tang, J. Deng, W. Li, O. I. Malyi, Y. Zhang, X. Zhou, S. Pan, J. Wei, Y. Cai, Z. Chen, X. Chen, *Adv. Mater.* **2017**, *29*, 1701828.

[32] Z. Tai, J. Yang, Y. Qi, X. Yan, Q. Xue, *RSC Adv.* **2013**, *3*, 12751.

[33] W. Kam, C. W. Liew, J. Y. Lim, S. Ramesh, *Ionics* **2013**, *20*, 665.

[34] H. Tian, G. Xu, B. Yang, G. Guo, *J. Food Eng.* **2011**, *107*, 21.

[35] X. Fu, L. Scudiero, W. H. Zhong, *J. Mater. Chem. A* **2019**, *7*, 1835.

[36] Z. Xue, D. He, X. Xie, *J. Mater. Chem. A* **2015**, *3*, 19218.

[37] J. Liu, Q. Zhang, T. Zhang, J. T. Li, L. Huang, S. G. Sun, *Adv. Funct. Mater.* **2015**, *25*, 3599.

[38] X. Fu, Y. Jewel, Y. Wang, J. Liu, W. H. Zhong, *J. Phys. Chem. Lett.* **2016**, *7*, 4304.

[39] C. Ying, X. Fu, W. H. Zhong, J. Liu, *J. Phys. Chem. Lett.* **2021**, *12*, 9429.

[40] H. J. Liang, Z. Y. Gu, X. X. Zhao, J. Z. Guo, J. L. Yang, W. H. Li, B. Li, Z. M. Liu, W. L. Li, X. L. Wu, *Angew. Chem.* **2021**, *60*, 26837.

[41] Y. C. Lu, A. N. Mansour, N. Yabuuchi, Y. Shao-Horn, *Chem. Mater.* **2009**, *21*, 4408.

[42] A. Ponrouch, D. Monti, A. Boschin, B. Steen, P. Johansson, M. R. Palacín, *J. Mater. Chem. A* **2015**, *3*, 22.

[43] C. Gao, J. Li, K. Sun, H. Li, B. Hong, M. Bai, K. Zhang, Z. Zhang, Y. Lai, *Chem. Eng. J.* **2021**, *412*, 128721.

[44] A. Zhao, T. Yuan, P. Li, C. Liu, H. Cong, X. Pu, Z. Chen, X. Ai, H. Yang, Y. Cao, *Nano Energy* **2022**, *91*, 106680.